

Magnetic Kronig-Penney model for Dirac electrons in single-layer graphene

M. Ramezani Masir

Departement Fysica, Universiteit Antwerpen Groenenborgerlaan 171, B-2020
Antwerpen, Belgium,
E-mail: mrmphys@gmail.com

P. Vasilopoulos

Department of Physics, Concordia University, Montreal, Quebec, Canada H3G 1M8.
E-mail: takis@alcor.concordia.ca

F. M. Peeters

Departement Fysica, Universiteit Antwerpen Groenenborgerlaan 171, B-2020
Antwerpen, Belgium,
Departamento de Física, Universidade Federal do Ceará, Caixa Postal 6030, Campus
do Pici, 60455-760 Fortaleza, Ceará, Brazil
E-mail: francois.peeters@ua.ac.be

Abstract. The properties of Dirac electrons in a magnetic superlattice (SL) on graphene consisting of very high and thin (δ -function) barriers are investigated. We obtain the energy spectrum analytically and study the transmission through a finite number of barriers. The results are contrasted with those for electrons described by the Schrödinger equation. In addition, a collimation of an incident beam of electrons is obtained along the direction perpendicular to that of the SL. We also highlight the analogy with optical media in which the refractive index varies in space.

1. Introduction

During the last five years single-layer graphene (a monolayer of carbon atoms) has become a very active field of research in nanophysics [1, 2]. It is expected that this material will serve as a base for new electronic and opto-electric devices. The reason is that graphene's electronic properties are drastically different from those, say, of conventional semiconductors. Charge carriers in a wide single-layer graphene behave like "relativistic", chiral, and massless particles with a "light speed" equal to the Fermi velocity and possess a *gapless, linear* spectrum close to the K and K' points. One major consequence is the perfect transmission through arbitrarily high and wide barriers, referred to as Klein tunneling.

One of the most challenging tasks is to learn how to control the electron behavior using electric fields in graphene. This task is made complicated precisely by the Klein tunneling according to which Dirac electrons in graphene can tunnel through arbitrarily wide and high electric barriers [3].

Alternatively, one can apply a magnetic field to control the electron motion. It was shown in numerous papers that an inhomogeneous magnetic field can confine standard electrons described by the Schrödinger equation [4, 5, 6]. The question then arises whether it can confine Dirac electrons in graphene. Up to now semi-infinite magnetic structures, that are homogeneous in one direction, were considered and made the task simpler by converting the problem into an one-dimensional (1D) one [7, 8, 9, 10, 11, 12, 13, 14, 15]. In particular, a magnetic confinement of Dirac electrons in graphene was reported in structures involving one [7] or several magnetic barriers [8, 9] as well as in superlattices, without magnetic field for some very special values of the parameters involved [16]. In such structures standard electrons can remain close to the interface and move along so-called snake orbits [5] or in pure quantum mechanical unidirectional states [4].

Given the importance of graphene, it would be appropriate to study this magnetic confinement more systematically. We make such a study here by considering a *magnetic* Kronig-Penney (KP) model in graphene, i.e., a series of magnetic δ -function barriers that alternate in sign. This model can be realized experimentally in two different ways:

- 1) One can deposit ferromagnetic strips on top of a graphene layer but in a way that there is no electrical contact between graphene and these strips. When one magnetizes the strips along the x direction, cf. Fig. 1(a), by, e.g., applying an in-plane magnetic field, the charge carriers in the graphene layer feel an inhomogeneous magnetic field profile. This profile can be well approximated [22] by $2B_0z_0h/d(x^2 + z_0^2)$ on one edge of the strip and by $-2B_0z_0h/(x^2 + z_0^2)$ on the other, where z_0 is the distance between the 2DEG and the strip, and d and h the width and height of the strip (see Fig. 1(b)). The resulting magnetic field profile will be modeled by two magnetic δ functions of height $2\pi B_0h$. Such ferromagnetic strips were deposited on top of a two-dimensional electron gas (2DEG) in a semiconductor heterostructure in Ref. [23].

- 2) It was recently shown that local strain in graphene induces an effective inhomogeneous

magnetic field [24] (Fig. 1(c)). When one puts the graphene layer on a periodically structured substrate the graphene at the edges of the substrate becomes strained and the situation can be described by a magnetic δ -function profile such as that shown in Fig. 2.

In a quantum mechanical treatment of the above two systems the vector potential $\mathbf{A}(x)$ is the essential quantity and, within the Landau gauge, $\mathbf{A}(x)$ is nothing else than a periodic array of step functions. The Hamiltonian describing this system is periodic and consequently we expect the energy spectrum of the charge carriers in graphene to exhibit a band structure. The advantage of this *magnetic Kronig-Penney* (KP) model is mainly its analytical simplicity that provides some insight and allows a contrast with the same model for standard electrons [27]. To do that we adapt a method developed in optics, for a media with periodic in space refractive index. This optical method is clear and very well suited to the problem. Incidentally, there are many analogues of optical behavior in electronics, such as focusing [17, 18, 19], collimation or quasi-1D motion of electrons and photons [16, 20, 4, 8], and interference [21] in a 2DEG.

The manuscript is organized as follows. In Sec. 2 we present the method and evaluate the spectrum and electron transmission through two antiparallel, δ -function magnetic barriers. In Sec. 3 we consider superlattices of such barriers and present numerical results for the energy spectrum. In Sec. 4 we consider a series of δ -function vector potentials and our concluding remarks are given in Sec. 5.

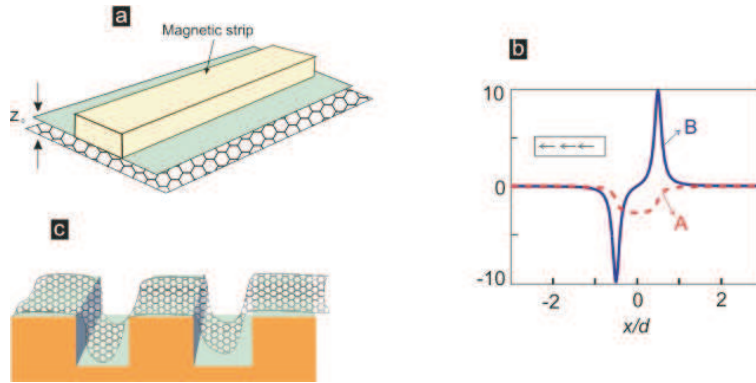


Figure 1. (a) Layout of the system: a ferromagnetic stripe on top of a bilayer graphene sheet separated by a thin oxide layer. (b) Magnetic field and corresponding vector potential at a distance $z_0 = 0.1$ under the stripe for parallel to it. (c) The graphene layer on top of a periodic structured surface.

2. Characteristic matrix for Dirac electrons

An electron in a single-layer graphene, in the presence of a perpendicular magnetic field $B(x)$, which depends on x , is adequately described by the Hamiltonian

$$H_0 = v_F \sigma \cdot (\mathbf{p} + e\mathbf{A}(x)), \quad (1)$$

where \mathbf{p} is the momentum operator, v_F the Fermi velocity, and $\mathbf{A}(x)$ the vector potential. To simplify the notation we introduce the dimensionless units: $\ell_B = [\hbar/eB_0]^{1/2}$, $B(x) \rightarrow B_0 B(x)$, $\mathbf{A}(x) \rightarrow B_0 \ell_B \mathbf{A}(x)$, $t \rightarrow t \ell_B / v_F$, $\vec{r} \rightarrow \ell_B \vec{r}$, $\vec{v} \rightarrow v_F \vec{v}$, $E \rightarrow E_0 E$, $u(x) \rightarrow E_0 u(x)$, $E_0 = \hbar v_F / \ell_B$. Here ℓ_B is the magnetic length and t the tunneling strength. In these units Eq. (1) takes the form

$$H = \begin{pmatrix} 0 & \partial_x - i\partial_y + A(x) \\ \partial_x + i\partial_y - A(x) & 0 \end{pmatrix}. \quad (2)$$

Then the equation $H\Psi(x, y) = E\Psi(x, y)$ admits solutions of the form

$$\Psi(x, y) = \begin{pmatrix} \psi_I(x, y) \\ \psi_{II}(x, y) \end{pmatrix}, \quad (3)$$

with $\psi_I(x, y), \psi_{II}(x, y)$ obeying the coupled equations

$$i \left[\frac{\partial}{\partial x} - i \frac{\partial}{\partial y} + A(x) \right] \psi_{II} + E \psi_I = 0, \quad (4)$$

$$i \left[\frac{\partial}{\partial x} + i \frac{\partial}{\partial y} - A(x) \right] \psi_I + E \psi_{II} = 0. \quad (5)$$

Due to the translational invariance along the y direction we assume solutions of the form $\Psi(x, y) = \exp i k_y y (U(x), V(x))^T$, with the superscript T denoting the transpose of the row vector. For $B(x) \sim \delta(x)$ the corresponding vector potential is a step function $A(x) \sim \Theta(x)$. For $A(x) = P$ constant, Eqs. (4) and (5) take the form

$$\left[\frac{d}{dx} + (k_y + P) \right] V = iEU, \quad (6)$$

$$\left[\frac{d}{dx} - (k_y + P) \right] U = iEV, \quad (7)$$

Equations (3)-(7) correspond to those for an electromagnetic wave propagating through a medium in which the refractive index varies periodically. The two components of $\Psi(x, y)$ correspond to those of the electric (or magnetic) field of the wave [28, 29]. Equations (6) and Eq. (7) can be readily decoupled by substitution. The result is

$$\frac{d^2 Z}{dx^2} + [E^2 - (k_y + P)^2] Z = 0, \quad (8)$$

where $Z = U, V$. If $E^2 \rightarrow E'$ and $(k_y + P)^2 \rightarrow V_{eff}$, Eq. (8) reduces to a Schrödinger equation for a standard electron where $V_{eff}(k_y, x) = (k_y + P)^2$ can be considered as an effective potential. Taking θ_0 as the angle of incidence, we have $k_x = E \cos \theta_0 = [E^2 - k_y^2]^{1/2}$ and $k_y = E \sin \theta_0$ are the wave vector components outside the medium and $k'_x = E \cos \theta = [E^2 - (k_y + P)^2]^{1/2}$ is the electron wave vector inside the medium and $\theta = \tan^{-1}(k_y/k'_x)$ is the refraction angle. This renders Eq. (8) simpler with acceptable solutions for U and V

$$U(x) = A \cos(Ex \cos \theta) + B \sin(Ex \cos \theta), \quad (9)$$

$$V(x) = -i \{ B \cos(\theta + Ex \cos \theta) - A \sin(\theta + Ex \cos \theta) \}. \quad (10)$$

For future purposes, we write U and V as a linear combination of U_1, U_2 and V_1, V_2 :

$$\begin{aligned} \frac{dV_1}{dx} + (k_y + P)V_1 &= iEU_1, & \frac{dV_2}{dx} + (k_y + P)V_2 &= iEU_2. \\ \frac{dU_1}{dx} - (k_y + P)U_1 &= iEV_1, & \frac{dU_2}{dx} - (k_y + P)U_2 &= iEV_2. \end{aligned} \quad (11)$$

We now multiply the equations of the first row by U_2 and U_1 , respectively, and those of the second by V_2 and V_1 . The resulting equations lead to

$$\frac{d\mathbf{D}}{dx} = U_1'V_2 + U_1V_2' - V_1'U_2 - V_1U_2' = 0, \quad (12)$$

where $\mathbf{D} = \det D$ and

$$D = \begin{pmatrix} U_1 & V_1 \\ U_2 & V_2 \end{pmatrix}. \quad (13)$$

Equation (12) shows that the determinant of the matrix (13) associated with any two arbitrary solutions of Eq. (8) is a constant, i.e, D is an invariant of the system of Eqs. (11). This also follows from the well-known property of the Wronskian of second-order differential equations. For our purposes the most convenient choice of particular solutions is

$$\begin{aligned} U_1 &= f(x), & U_2 &= F(x), \\ V_1 &= g(x), & V_2 &= G(x), \end{aligned} \quad (14)$$

such that

$$f(0) = g(0) = 0, \quad F(0) = G(0) = 1. \quad (15)$$

Then the solution with $U(0) = U_0$, $V(0) = V_0$, can be expressed as

$$U = FU_0 + fV_0, \quad V = GU_0 + gV_0 \quad (16)$$

or, in matrix notation, as

$$\mathbf{Q} = \begin{bmatrix} U(x) \\ V(x) \end{bmatrix}, \quad \mathbf{Q}_0 = \begin{bmatrix} U_0 \\ V_0 \end{bmatrix}, \quad \mathbf{N} = \begin{bmatrix} F(x) & f(x) \\ G(x) & g(x) \end{bmatrix}. \quad (17)$$

Since D is constant, the determinant of the square matrix N is a constant; its value, found by setting $x = 0$, is $\det N = Fg - fG = 1$. It is usually more convenient to express U_0 and V_0 as a function of $U(x)$ and $V(x)$. Solving for U_0 and V_0 we obtain $\mathbf{Q}_0 = \mathbf{M}\mathbf{Q}$, where

$$\mathbf{M} = \begin{bmatrix} g(x) & -f(x) \\ -G(x) & F(x) \end{bmatrix}. \quad (18)$$

This matrix \mathbf{M} is unimodular, $|\mathbf{M}| = 1$. Now we can find the characteristic matrix from Eqs. (9) and (10) as

$$\mathbf{M}(x) = \frac{1}{\cos \theta} \begin{bmatrix} \cos(\theta + Ex \cos \theta) & -i \sin(Ex \cos \theta) \\ -i \sin(Ex \cos \theta) & \cos(\theta - Ex \cos \theta) \end{bmatrix}. \quad (19)$$

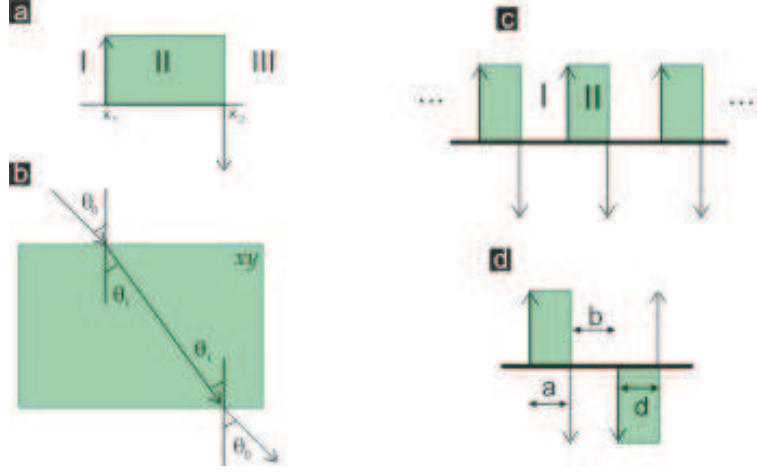


Figure 2. (a) Two opposite magnetic δ -function barriers, indicated by arrows (top figure) the vector potential showed by shaded (green) area. (b) The angles related to the propagation of an electron through this system (is shown in the bottom figure). (c) Schematics of a periodic vector potential (shaded areas) and corresponding magnetic field indicated by the black arrows. (d) Arrangement of magnetic δ -functions that leads to a periodic area of vector potential with alternating sign.

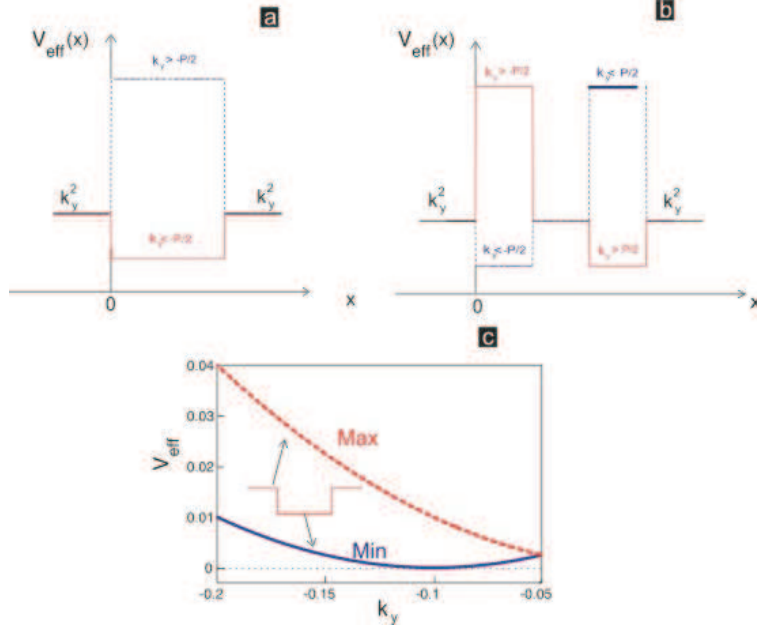


Figure 3. The effective potential for $k_y < -P/2$ and $k_y > P/2$ for two different cases, (a) vector potential with non-zero average corresponding to Fig. 2(a), and (b) vector potential with zero average corresponding to Fig. 2(c). (c) Minimum (blue full curve) and maximum (red dashed curve) of the effective potential vs k_y corresponding to the situation depicted in (a) for $P = 0.1$.

2.1. Bound states

Regards to the average of vector potential we shall consider two different systems: one with zero average and the other with non zero average along the x -direction. First let us consider the magnetic field profile as shown in Fig. 2(a) for which the corresponding vector potential is

$$A(x) = P\Theta(x)\Theta(L - x), \quad (20)$$

where $\Theta(x) = 0(x < 0)$, $1(x > 0)$ is the theta function. This vector potential has a non-zero average, and the corresponding effective potential becomes (see Fig. 3(a)) as

$$V_{eff}(k_y, x) \sim \begin{cases} k_y^2 & x < 0 \\ (k_y + P)^2 & 0 < x < L \\ k_y^2 & x > L \end{cases} . \quad (21)$$

Here L is measured in the unit of magnetic length l_B . There are two different cases which we have to consider.

Case 1 for $k_y < -P/2$: as shown in Fig. 3(a) by the full red curve, we have a 1D symmetric quantum well which, as is well-known, has at least one bound state (see also Fig. 3(c)). For $E^2 < k_y^2$ the particle will be bound while for $E^2 > k_y^2$ we have scattered states, or equivalently the electron tunnels through the magnetic barriers.

Case 2 for $k_y > -P/2$: as shown in Fig. 3(a) by the dotted blue curve, the effective potential is like a barrier. We have a pure tunneling problem. With reference to Fig. 2, $x_1 = 0$ and $x_2 = L$, the solutions are as follows. For $x < 0$ the wave function is

$$\psi(x) = Ce^{\kappa x} \begin{pmatrix} 1 \\ -ie^{-\xi} \end{pmatrix}, \quad (22)$$

where $\kappa = E \cosh \xi$ and $k_y = E \sinh \xi$, while for $x > L$ it is

$$\psi(x) = De^{-\kappa x} \begin{pmatrix} 1 \\ ie^{\xi} \end{pmatrix}. \quad (23)$$

In the middle region, $0 < x < L$, the wave function is given by

$$\psi(x) = Fe^{ik'x} \begin{pmatrix} 1 \\ e^{i\theta} \end{pmatrix} + Qe^{-ik'x} \begin{pmatrix} 1 \\ -e^{-i\theta} \end{pmatrix}. \quad (24)$$

With $k' = [E^2 - (k_y + P)^2]^{1/2} = E \cos \theta$. Matching the wave functions at $x = 0$ and $x = L$ leads to a system of four equations relating the coefficients C , D , F , and Q . Setting the determinant of these coefficients equal to zero, we obtain the transcendental equation, the solution of it gives the energy spectrum

$$\cos \theta \cosh \xi \cos k'L + \sin \theta \sinh \xi \sin k'L = 0. \quad (25)$$

For the special value of $k_y = -P$, $\sin \theta = 0$, and we can rewrite Eq. (25) as $\cos(EL) = 0$ or equally $E_n = \left(n + \frac{1}{2}\right) \frac{\pi}{L}$. The resulting bound states, as a function of k_y , are shown by the red full curves in Fig. 4(a). The area of existence of bound states is delimited by the lines $E = -k_y$ and $E = -(k_y + P)$. The number of bound states increases with

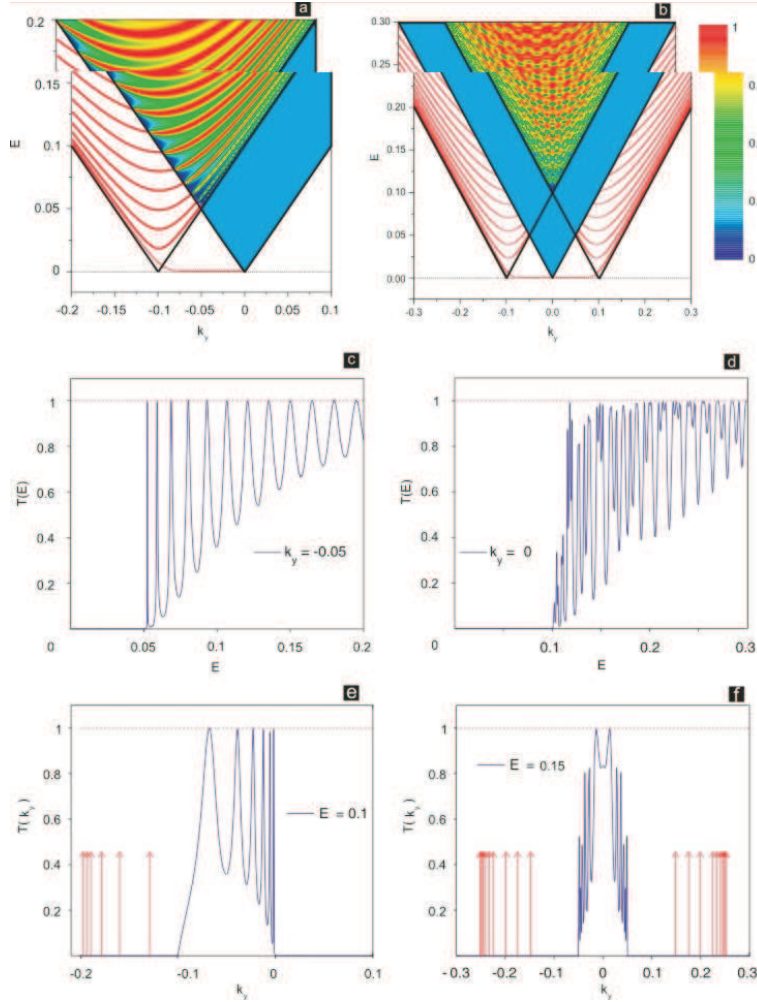


Figure 4. (a) Energy spectrum (red full curves on white background) and contour plot of the transmission (color background) through two magnetic, but with opposite direction δ -function barriers for $L = 200$ and $P = 0.1$. (b) the same as (a) but now for the configuration shown in Fig. 2(b) for $a = b = c = 200$ and $P = 0.1$. (c) Transmission vs energy through the magnetic δ -function barriers of in (a) $k_y = -0.05$. (d) same as (c) but now for the configuration shown in Fig. 2(b) for $k_y = 0$. (e) Transmission vs k_y through the system described in (a) for fixed $E = 0.1$. The red arrow lines indicate the position of the bound states. (f) same as (e) but now for the configuration shown in Fig. 2(b) for $E = 0.15$

$|k_y|$ which is also clear from the behavior of the min. and max. of the effective potential (see Fig. 3(c)). No bound states are found for $k_y > -P/2$ as is also apparent from Fig. 3(c). For $k_y \rightarrow -P/2$ the potential is shallow and only one bound state exists. The average velocity $v_n(k_y)$ along the y direction is given by

$$v_n(k_y) = \partial E / \partial k_y = \int_{-\infty}^{+\infty} dx j_y(x), \quad (26)$$

where $j_y = -i(U^*V - V^*U)$. From Fig. 4(a) it is clear that these bound states move along the y -direction, i.e. along the magnetic barriers. Their velocity $v_y > -v_F$ is

negative for $k_y < -P$ but as the electron is approaching $k_y \rightarrow -P$ we have $v_y \rightarrow 0$. For $k_y > -P$ the velocity $v_y > v_F$ is positive. This can be understood from the maximum and minimum of the effective potential which is shown in Fig. 3(c). The energy bound states can only exist between these two lines. Notice that the slope of $\min V_{eff}$ is negative for $k_y < -P$ while it turns positive for $k_y > -P$ which explains the k_y dependence of the velocity. From Fig. 4(a) it is clear there are two different classes of bound states. The bound state which follows very closely the $k_y = -P$ curve and extends to the region $-P < k_y < 0$ with energy close to zero has a wavefunction that is concentrated around the position of the two magnetic delta function and decays exponentially in the region $0 < x < L$. The wave function of the other bound states are concentrated in a region between the two magnetic delta-functions (i.e. like in a standing wave fashion) and decays exponentially outside this region.

Next, we consider a structure with zero-average vector potential as shown in Fig. 2(b), with corresponding effective potential shown in Fig. 3(b). The effective potential for $k_y < -P/2$ and $k_y > P/2$, consist of a potential well and a potential barrier and therefore has at least one bound state. Thus we expect bound states for all k_y with energy between $E = -(+)(k_y + P)$ and $E = -(+)k_y$ when $k_y < -P/2$ ($k_y > P/2$). The dispersion relation for those bound states are the solution of

$$M_{21} - M_{12} - iM_{22}e^{-\xi} - iM_{11}e^{\xi} = 0, \quad (27)$$

where \mathbf{M} is the transfer matrix for the unit shown in Fig. 2(d). These bound states are shown by the red full curves in Fig. 4(b). Because of the spatial inversion symmetry of the vector potential the spectrum has the symmetry $E(-k_y) = E(k_y)$. Notice that for $-P < k_y < P$ the lowest bound state has energy $E \approx 0$. For $-P/2 < k_y < P/2$ we have two potential barriers and therefore no bound states.

2.2. Reflection and transmission coefficients

Consider a plane wave incident upon a system of two δ -function magnetic barriers, identical in height but opposite in direction, placed at $x = 0$ and $x = L$, as shown schematically in Fig. 2(a). In this case the vector potential is constant for $0 \leq x \leq L$, zero outside this region, and homogeneous in the y direction. Below we derive expressions for the amplitudes and intensities of the reflected and transmitted waves.

Let A , R , and T denote the amplitudes of the incident, reflected, and transmitted waves, respectively. Further, let θ_0 be the angle of incidence and exit as shown in Fig. 2(b). The boundary conditions give

$$\begin{aligned} U_0 &= A + R, & U(L) &= Te^{ikL}, \\ V_0 &= Ae^{i\theta_0} - Re^{-i\theta_0}, & V(L) &= e^{i\theta_0}e^{ikh}T. \end{aligned} \quad (28)$$

The four quantities U_0, V_0, U , and V given by Eqs. (28) are connected by the basic relation $\mathbf{Q}_0 = \mathbf{M}\mathbf{Q}$; hence, with $J = m'_{11} + m'_{12}e^{i\theta_0}$ and $K = m'_{21} + m'_{22}e^{i\theta_0}$, we have

$$\begin{aligned} A + R &= JTe^{ikL}, \\ Ae^{i\theta_0} - Re^{-i\theta_0} &= KTe^{ikL}, \end{aligned} \quad (29)$$

where m'_{ij} are the elements of the characteristic matrix of the medium, evaluated at $x = L$. From Eq. (29) we obtain the reflection and transmission amplitudes

$$r = \frac{R}{A} = \frac{Je^{i\theta_0} - K}{Je^{-i\theta_0} + K}, \quad t = \frac{T}{A} = \frac{2e^{-ikh} \cos \theta_0}{Je^{-i\theta_0} + K}. \quad (30)$$

In terms of r and t the *reflectivity* and *transmissivity* are

$$\mathcal{R} = |r|^2, \quad \mathcal{T} = |t|^2. \quad (31)$$

The characteristic matrix for a homogeneous vector potential is given by Eq. (19). Labeling with subscripts 1, 2, and 3 quantities which refer to the regions, respectively, I, II, and III of Fig. 2(a), and by $L = x_2 - x_1$ distance between the magnetic δ -functions, we have ($\beta = EL \cos \theta_i$)

$$\begin{aligned} m'_{11} &= \cos(\theta_i + \beta) / \cos \theta_i, & m'_{22} &= \cos(\theta_i - \beta) / \cos \theta_i, \\ m'_{12} &= -i \sin \beta / \cos \theta_i, & m'_{21} &= -i \sin \beta / \cos \theta_i. \end{aligned} \quad (32)$$

The reflection and transmission amplitudes r and t are obtained by substituting these expressions in those for J and K that appear in Eq. (30). The resulting formula can be expressed in terms of the amplitudes r_{12}, t_{12} and r_{23}, t_{23} associated with the reflection at and transmission through the first and second "interface", respectively. We have

$$r_{12} = \frac{e^{i\theta_0} - e^{i\theta_i}}{e^{-i\theta_0} + e^{i\theta_i}}, \quad t_{12} = \frac{2 \cos \theta_0}{e^{-i\theta_0} + e^{i\theta_i}}, \quad (33)$$

and similar expressions for r_{23} and t_{23} . In terms of these expressions r and t become

$$r = \frac{r_{12} + r_{23}e^{2i\beta}}{1 + r_{12}r_{23}e^{2i\beta}}, \quad t = \frac{t_{12}t_{23}e^{i\beta}}{1 + r_{12}r_{23}e^{2i\beta}}. \quad (34)$$

The amplitude t of the transmission through the system is given by [8, 9, 12, 24],

$$t = \frac{2e^{-ikL} \cos \theta_0 \cos \theta_i}{e^{-i\beta}[\cos(\theta_0 + \theta_i) + 1] + e^{i\beta}[\cos(\theta_0 - \theta_i) - 1]}, \quad (35)$$

where $k_y = E \sin \theta_0$, and $k_y + P = E \sin \theta_i$. This equation remains invariant under the changes $E \rightarrow -E$, $\theta_0 \rightarrow -\theta_0$, $\theta_i \rightarrow -\theta_i$. A contour plot of the transmission is shown in Fig. 4(a) and slices for constant k_y and E are shown respectively in Fig. 4(c) and Fig. 4(d). By imposing the condition that the wave number k_x be real for incident and transmitted waves, we find that the angles θ_0 and θ_i are related by

$$\sin \theta_0 + P/E = \sin \theta_i. \quad (36)$$

Equation (36) expresses the angular confinement of the transmission elaborated in Refs. [8], [12], [26], and [9]. Notice its formal similarity with Snell's law. Using Eq. (36) we obtain the range of incidence angles θ_0 for which transmission through the first magnetic barrier is possible

$$-1 - P/E \leq \sin \theta_0 \leq 1 - P/E. \quad (37)$$

For the special value of the energy $E = P/2$ and θ_0 in the range $-\pi/2 \leq \theta_0 \leq \pi/2$, we have $\theta_i = \pi/2$ while for $E = -P/2$ the result is $\theta_i = -\pi/2$. Alternatively, we can put $\theta_i = \pm\pi/2$ in Eq. (36) and obtain, for $P > 0$, the result

$$\sin \theta_0^\pm = \pm 1 - P/E, \quad (38)$$

where the $+$ ($-$) sign corresponds to $E > 0$ ($E < 0$). A contour plot of the transmission as function of E and k_y , obtained from Eq. (35), is shown in Fig. 4(a). In Fig. 4(a) we distinguish three different regions. In the region between $E = -(k_y + P/2)$ and $E = -k_y$, the wave vector of the incident wave is imaginary and they are evanescent waves. In this region k' is real and it is possible to find localized states. The k and k' for the second region between $E = k_y + P/2$ and $E = -(k_y - P/2)$ are real and the electron can tunnel through the magnetic δ -barriers. In the blue shadow region between $E = k_y + P/2$ and $E = k_y - P/2$, k is real but k' is imaginary and solutions inside the barrier are evanescent and there is very little tunneling which becomes very quickly zero. The transmission probability $|T| = t \cdot t^*$ is equal to 1 for $\cos(2\beta) = 1$. In this case the energy becomes

$$E_n = \pm \left[n^2 \pi^2 / L^2 + (k_y + P)^2 \right]^{1/2}, \quad n = 1, 2, \dots \quad (39)$$

The condition $\cos(2\beta) = 1$, or equivalently $\beta = n\pi = E h \cos \theta_2$ with n an integer, should be combined with that for the transmission to occur in the region delimited by the curves $E = \pm(k_y + P)$ and $E = \pm k_y$. For example, in Fig. 4(a) for $k_y = -0.05$ and $0 < E < 0.2$ we have 12 maxima. It is readily seen that with these parameters in Eq. (39) we find 12 different energies as shown in Fig. 4(c).

Fig. 4(b) shows a contour plot of the transmission for the structure shown in Fig. 2(d), which is symmetric around $k_y = 0$. Notice that the number of resonances has increased substantially as compared to previous case which is due to the fact that we have twice as many magnetic barriers in our systems.

3. A series of units with magnetic δ -function barriers

3.1. N units

We consider a system of N units, such as those shown in Fig. 2(a) and Fig. 2(d) with periods $L = a + b$ and $L = a + b + c + d$, respectively. The corresponding periodic vector potential is $\mathbf{A}(x) = \mathbf{A}(x + nL)$ and the magnetic field $\mathbf{B} = \mathbf{B}(x + nL)$, with $n = 1, 2, \dots, N$. The characteristic matrix for one period $\mathbf{M}(L)$ is denoted by

$$\mathbf{M}(L) = \begin{bmatrix} m_{11} & m_{12} \\ m_{21} & m_{22} \end{bmatrix}. \quad (40)$$

On account of the periodicity we have

$$\mathbf{M}(NL) = \underbrace{\mathbf{M}(L) \cdot \mathbf{M}(L) \dots \mathbf{M}(L)}_{N \text{ factors}} = (\mathbf{M}(L))^N. \quad (41)$$

To evaluate the elements of $\mathbf{M}(NL)$ we use a result from the theory of matrices, according to which the N th power of a unimodular matrix $\mathbf{M}(L)$ is ($u_N(\chi) \equiv u_N$)

$$[\mathbf{M}(L)]^N = \begin{bmatrix} m_{11}u_{N-1} - u_{N-2} & m_{12}u_{N-1} \\ m_{21}u_{N-1} & m_{22}u_{N-1} - u_{N-2} \end{bmatrix}, \quad (42)$$

with $\chi = \frac{1}{2} \text{Tr } \mathbf{M}$ and u_N the Chebyshev polynomials of the second kind:

$$u_N(\chi) = \sin[(N+1)\zeta] / \sin \zeta, \quad (43)$$

where

$$\zeta = \cos^{-1} \chi, \quad (44)$$

Here ζ is the *Bloch phase* of the periodic system [33], which is related to the eigenfunctions of \mathbf{M} . In the limit case of $N \rightarrow \infty$, we have total reflection when ζ is outside the range $(-1, 1)$.

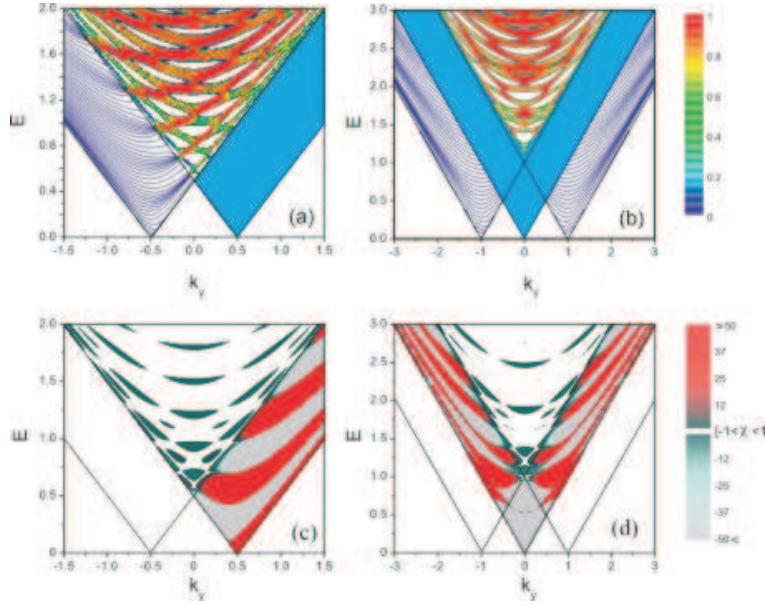


Figure 5. Contour plot of the transmission (a) and Bloch phase (c) through $N = 10$ magnetic δ -function barriers with $a = 10$, $b = 10$, and $P = 1$. (b) and (d) The same as in (a) and (c) for $a = 5$, $b = 5$, $c = 5$, $d = 5$, and $P = 1$, single unit.

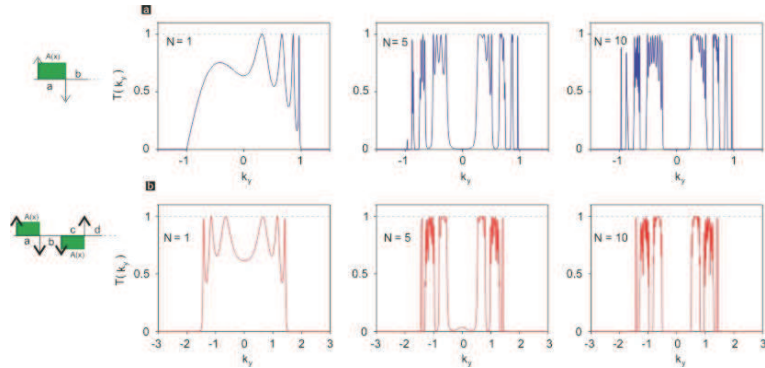


Figure 6. (a) and (b) Transmission vs energy through $N = 1, 5, 10$ magnetic units of δ -function barriers shown on the left. The upper unit has $a = 10$, $b = 10$, $P = 1$, $E = 1.5$ and the bottom one $a = b = c = d = 5$, and $P = 1$ and $E = 2.5$.

3.2. Superlattice

Here we consider a finite number N of lattice unit shown in Fig. 2(c). We set

$$\begin{aligned} \beta_2 &= Eb \cos \theta_2, \quad \beta_1 = Ea \cos \theta_1, \quad p_2 = 1/\cos \theta_2, \\ p_1 &= 1/\cos \theta_1, \quad h = a + b, \quad \lambda_n^\pm = \theta_n \pm \beta_n. \end{aligned} \quad (45)$$

The characteristic matrix $\mathbf{M}_2(L)$ for one period is readily obtained, in terms of these quantities, as in Sec. II, and from that the characteristic matrix $\mathbf{M}_{2N}(NL)$ of the multilayer system according to Eq. (41). Its elements are

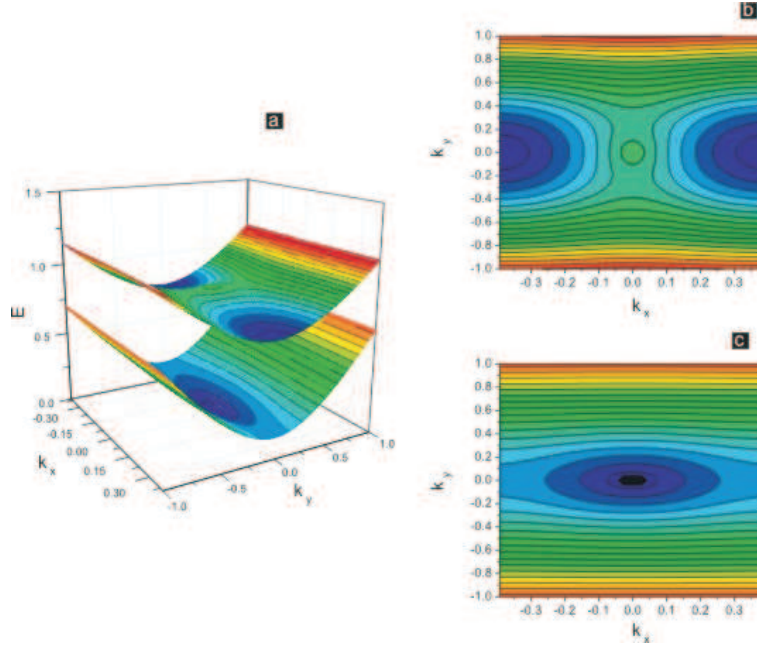


Figure 7. (a) The first two energy bands and contour plot of second (b) and first (c) band for a magnetic SL of δ -function barriers with $a = 4$, $b = 4$, and $P = 1$.

$$\begin{aligned} M_{11} &= s[\cos \lambda_2^+ \cos \lambda_1^+ - \sin \beta_2 \sin \beta_1]u_{N-1} - u_{N-2}, \\ M_{12} &= -is[\cos \lambda_2^+ \sin \beta_1 + \sin \beta_2 \cos \lambda_1^-]u_{N-1}, \\ M_{21} &= -is[\cos \lambda_1^+ \sin \beta_2 + \sin \beta_1 \cos \lambda_2^-]u_{N-1}, \\ M_{22} &= s[\cos \lambda_2^- \cos \lambda_1^- - \sin \beta_2 \sin \beta_1]u_{N-1} - u_{N-2}, \end{aligned} \quad (46)$$

where $s = p_2 p_1$, $u_N \equiv u_N(\chi)$, and

$$\chi = \cos(k_1 a) \cos(k_2 b) - \left(\frac{k_2^2 + k_1^2 + P^2}{2k_2 k_1} \right) \sin(k_1 a) \sin(k_2 b). \quad (47)$$

The reflection and transmission coefficients of the multi-unit system are immediately obtained by substituting these expressions into Eq. (30). The numerical results are shown in Figs. 5, 6 for finite superlattice with $N = 10$ units. Two different type of structures are considered as shown in the insets to Figs. 6. The transmission doesn't have $k_y \rightarrow -k_y$ symmetry for the periodic system with magnetic delta up-down as is

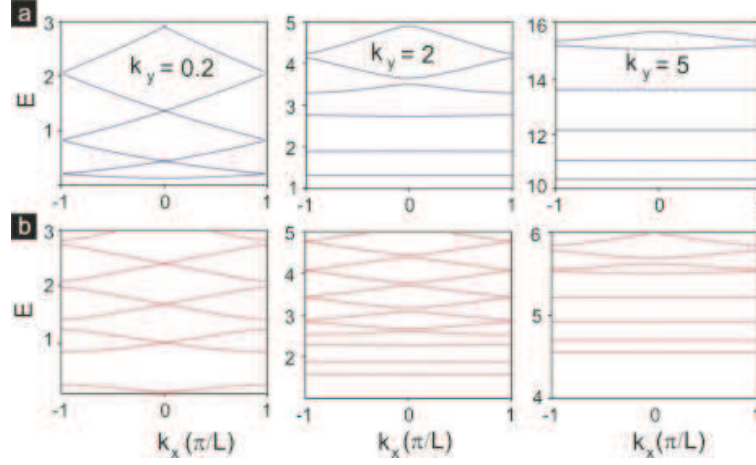


Figure 8. Dispersion relation (E vs k) for a standard electron in (a) and a Dirac electron in (b). The fixed values of k_y are shown in the panels and $L = 8$ and $P = 1$ (the energy for standard electron is measured in units of $\hbar\omega_c$ with $\omega_c = \sqrt{eB_0/mc}$ and all distances in $l_B = \sqrt{\hbar c/eB_0}$).

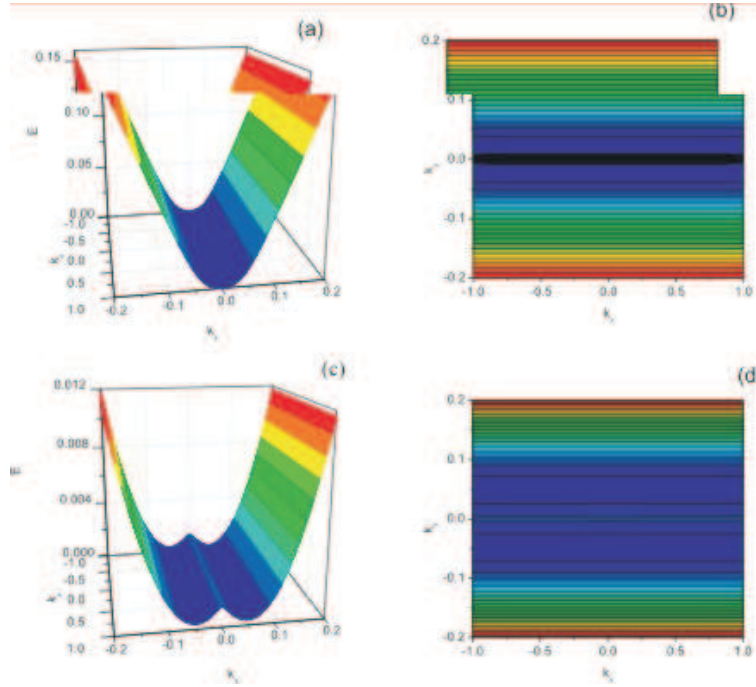


Figure 9. First energy band for (a) standard and (c) Dirac electron in SL of magnetic δ -function barriers with $a = 100$, $b = 100$, and $P = 0.1$. (b) and (d) corresponding contour plots of (a) and (c) (the energy for standard electron is measured in units of $\hbar\omega_c$ with $\omega_c = \sqrt{eB_0/mc}$ and all distances in $l_B = \sqrt{\hbar c/eB_0}$).

apparent from Fig. 6(a). We contrast these results with the case in which we used an arrangement of magnetic *delta*-function as in previous structure plus another unit with opposite direction of magnetic delta function. As is clearly shown in Fig. 6(b), we

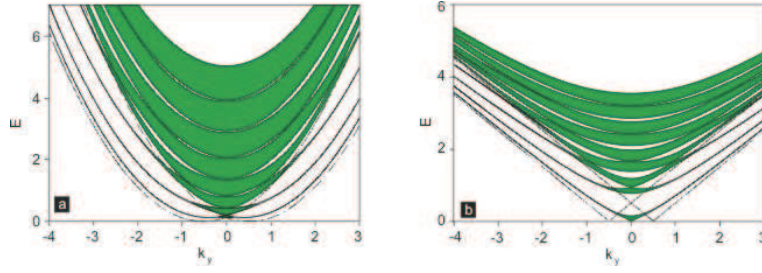


Figure 10. Dispersion relation for a (a) standard electron and a (b) Dirac electron. The period is $L = a + b = 8$ and the shaded (in green) regions are the lowest six allowed bands. The solid curves in both panels, the dash-dotted curves in (a) and the dashed ones in (b) show bound states for free electron (the energy for standard electron is measured in units of $\hbar\omega_c$ with $\omega_c = \sqrt{eB_0/mc}$ and all distances in $l_B = \sqrt{c\hbar/eB_0}$).

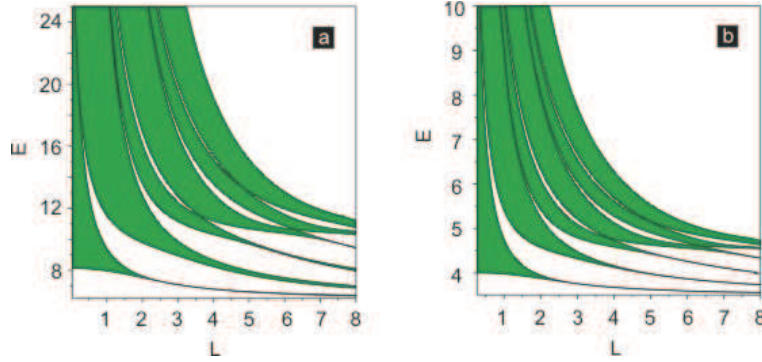


Figure 11. Energy vs period $L = a + b$ for (a) standard electron and (b) Dirac electron with fixed $k_y = 4$ (the energy for standard electron is measured in units of $\hbar\omega_c$ with $\omega_c = \sqrt{eB_0/mc}$ and all distances in $l_B = \sqrt{c\hbar/eB_0}$).

have $k_y \rightarrow -k_y$ symmetry for the transmission probability through this structure. The transmission resonances are more pronounced, i.e., the dips become deeper, when the number of barriers increases for both types of units. But the gaps occur when the wave is mostly reflected. The position of these gaps, which are especially pronounced as N increases, can also be found from the structure of the Bloch phase ζ , as shown in Figs. 5(c) and (d). In Fig. 5 the bound states are shown by the blue solid curves that are situated in the area $-k_y - P/2 < E < -k_y + P/2$ in case (a) and in $-k_y - P/2 < E < -k_y$ for case (b) plus an area located symmetric with respect to k_y . Notice in Fig. 5(a) that several bound states merge into a resonant states at $E = -k_y + P/2$. This is different from Fig. 4(a) where each bound state becomes a resonant state at $E = -k_y$.

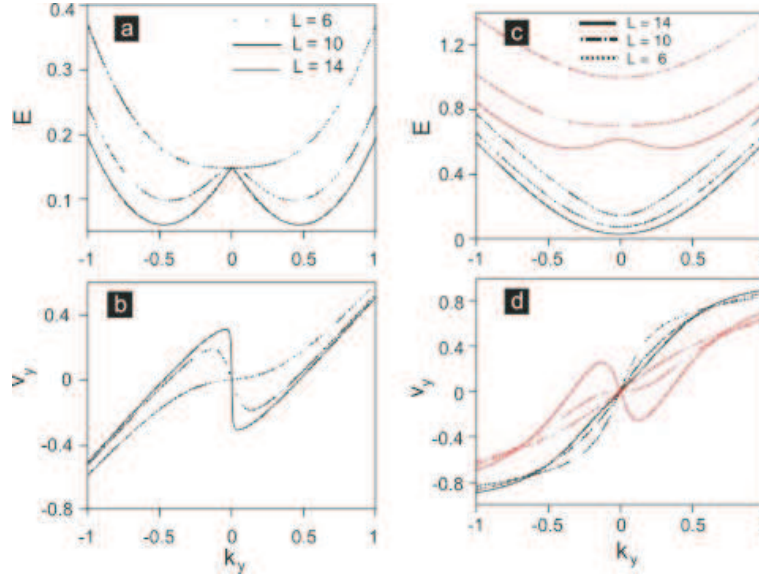


Figure 12. (a) and (b): Lowest-energy band for a standard electrons and drift velocity vs k_y for three different values of L . (c) and (d): First (black curves) and second (red curves) band for Dirac electrons and the drift velocity vs k_y for three different values of L (the energy for standard electron is measured in units of $\hbar\omega_c$ with $\omega_c = \sqrt{eB_0/mc}$ and all distances in $l_B = \sqrt{\hbar c/eB_0}$).

3.3. Spectrum of a superlattice

Lets take $N \rightarrow \infty$. We can find the energy-momentum relation from the previous standard calculation [32, 33] by using

$$\cos(k_x L) = \frac{1}{2} \text{Tr } \mathbf{M} = \chi, \quad (48)$$

where M is the characteristic matrix of one period, which results into

$$\cos(k_1 a) \cos(k_2 b) - \left(\frac{k_2^2 + k_1^2 + P^2}{2k_2 k_1} \right) \sin(k_1 a) \sin(k_2 b) = \cos k(b + a). \quad (49)$$

With reference to the regions I and II shown in Fig. 2(a), we write $k_1 = [E^2 - k_y^2]^{1/2}$ and $k_2 = [E^2 - (k_y + P)^2]^{1/2}$ and show the solution for $E^2 > (k_y + P)^2$ in Fig. 9. Differences of Eq. (49) from the corresponding result of Ref. [27], Eq. (7), for the case of Schrödinger electrons, is the term P^2 in the prefactor of the second term on the right-hand side and the linear E vs k spectrum instead of the quadratic one in Ref. [27]. If P is large the differences become more pronounced. Our numerical results for the energy spectrum are shown in Figs. 7, 8, 9, 10, and 11. The results for standard and Dirac electrons show similarities but also important differences. The first band shows a qualitative difference near $k_y \approx 0$, see Fig. 9. As Figs. 7, 9(a) and 9(b) show, the band behavior in the $k = k_x$ direction for fixed k_y is constant and almost symmetric about $k_y = 0$; the motion becomes nearly 1D for relatively large k_y . From the contour plots of Figs. 9(b) and (d), as well as from Fig. 7(c), we infer a collimation along the k_y direction, i.e., $v_y \propto \partial E / \partial k_y \approx v_F$ and $v_x \approx 0$, which is similar to that found for a SL of

electric potential barriers [16] for some specific values of the barrier heights. Also there are no gaps for $k_y \approx 0$ in Fig. 10(a) but there are for the case of Dirac electrons as seen in Fig. 10(b). This difference can be traced back to the presence of P^2 in the dispersion relation Eq. (49) when compare to the same equation for the standard electron. The even-number energy bands in Fig. 11(b) are wider than those in Fig. 11(a) and, as a function of the period, the energy decreases faster for Dirac electrons. This behavior of the bands for Dirac electrons is very similar to that for the frequency ω vs k_y or L in media with a periodically varying refractive index [29]. This is clearly a consequence of the linear $E - k$ relation. Notice the differences between the lowest bands shown in panels (a) and (b) in Fig. 12 and in particular the difference between the corresponding drift velocities as functions of k_y .

4. A series of δ -function vector potentials

In the limit that the distance between the opposite directed magnetic barriers decrease to zero the vector potential approaches a δ -function [24]. We consider a series of magnetic δ -function vector potentials $A(x) = \sum_{n=-\infty}^{\infty} A_0 \delta(x - nL)$ as shown in Fig. 11(a). First we consider a single such potential, that is zero everywhere except at $x = 0$. We start with Eqs. (6) and (7) which becomes now

$$-i [d/dx + k_y + \ell_B A_0 \delta(x)] \phi_b = E \phi_a, \quad (50)$$

$$-i [d/dx - k_y - \ell_B A_0 \delta(x)] \phi_a = E \phi_b. \quad (51)$$

The solutions are readily obtained in the form

$$\phi_a = \begin{cases} A \cos(\varepsilon x \cos \theta) + B \sin(\varepsilon x \cos \theta), & x < 0, \\ C \cos(\varepsilon x \cos \theta) + D \sin(\varepsilon x \cos \theta), & x > 0, \end{cases} \quad (52)$$

$$\phi_b = \begin{cases} -i \{B \cos(\theta + \varepsilon x \cos \theta) - A \sin(\theta + \varepsilon x \cos \theta)\}, & x < 0, \\ -i \{D \cos(\theta + \varepsilon x \cos \theta) - C \sin(\theta + \varepsilon x \cos \theta)\}, & x > 0. \end{cases} \quad (53)$$

Integrating Eqs. (50), (51) around 0 gives

$$-i \int_{0^-}^{0^+} [d/dx + (k_y + \ell_B A_0 \delta(x))] \phi_b dx = E \int_{0^-}^{0^+} \phi_a dx, \quad (54)$$

$$-i \int_{0^-}^{0^+} [d/dx - (k_y - \ell_B A_0 \delta(x))] \phi_a dx = E \int_{0^-}^{0^+} \phi_b dx \quad (55)$$

and

$$\phi_b(0^-) = \eta \phi_b(0^+), \quad \phi_a(0^+) = \eta \phi_a(0^-). \quad (56)$$

We now consider the entire series of δ -function vector potentials shown in Fig. 13(a) and use Eqs. (54) and the periodic boundary condition $\Psi_I(0) = e^{ik_x L} \Psi_{II}(L)$. The resulting dispersion relation for the superlattice is

$$\cos(kL) = 2\eta(1 + \eta^2)^{-1} \cos(k_x L), \quad (57)$$

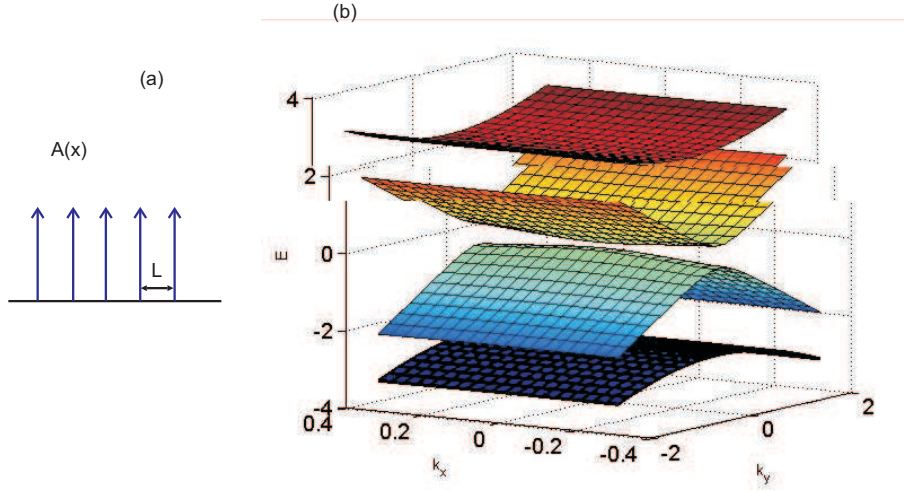


Figure 13. (a) A series of δ -function vector potentials. (b) Dispersion relation for the system shown in (a).

where $\eta = 1 + \ell_B A_0$. From Eq. (57) we can find the energy spectrum as

$$E_n(k_x, k_y) = \pm \sqrt{2n\pi + k_y^2 + \left(\frac{1}{L} \cos^{-1} \left(\frac{2\eta}{1 + \eta^2} \cos(k_x L) \right) \right)^2}; \quad (58)$$

We can define

$$(1/L) \cos^{-1} \left[2\eta(1 + \eta^2)^{-1} \cos(k_x L) \right] = s, \quad (59)$$

and obtain

$$E = \pm [2n\pi + k_y^2 + s^2]^{1/2}. \quad (60)$$

The energy bands around the Dirac point are plotted in Fig. 12(b). Notice that: 1) there is an opening of a gap at the Dirac point, 2) the motion is strongly 1D, i.e. along the k_y -direction, and 3) higher subbands have a smaller dispersion.

5. Concluding remarks

We developed a *magnetic* Kronig-Penney model for Dirac electrons in graphene. The model is essentially a series of very high and very narrow *magnetic* δ -function barriers alternating in signs. The treatment of the transmission through such a series of barriers followed closely the one developed in optics for media in which the refractive index varies in space [28, 29]. We contrasted a few of the results with those for standard electrons described by the Schrödinger equation [27].

In several cases the energy spectrum or the dispersion relation were obtained analytically, cf. Eqs. (25), (39), (47), (48), and (57), largely due to the simplicity of the model and the adapted method from optics. For only two *magnetic* δ -function barriers, opposite in sign, we saw several bound states, whose number increases with $|k_y|$, and a reduction of the wavevector range for which tunneling is possible, cf. Fig.

4(a). This is in line with that reported earlier for single [7] and multiple [9] barriers. The reduction becomes stronger as we increase the number of barriers, cf. Fig. 4(b). We also made contact with Snell's law in optics, cf. Eq. (36): the term P/E represents the deviation from this law.

An important feature of the superlattice results is a collimation of an incident electron beam normal to the superlattice direction at least for large wave vectors. As easily seen from Figs. 7 and 8, for $|k_y| \geq 2$ we have $v_x \propto \partial E / \partial k_x \approx 0$ for the first three minibands in the middle panels and nearly five minibands in the right panels. This occurs for both standard electrons and Dirac electrons but notice an important difference for $|k_y| \approx 0$ shown clearly in Fig. 9. This collimation is similar to that reported in Ref. [16] for superlattices involving only electric barriers but with somewhat unrealistic large barrier heights.

It is also worth emphasizing the differences and similarities in the first two minibands and the corresponding drift velocities as functions of k_y for different periods L and constant k_x as shown in Fig. 12. Notice in particular the resemblance between the drift velocities in the lowest miniband for standard electrons and the second miniband for Dirac electrons.

Given that ferromagnetic strips were successfully deposited on top of a 2DEG in a semiconductor heterostructure [23], we hope they will be deposited on graphene too and that the results of this paper will be tested in a near future.

ACKNOWLEDGEMENTS

We thank Prof. A. Matulis for helpful discussions. This work was supported by the Flemish Science Foundation (FWO-VI), the Belgian Science Policy (IAP), the Brazilian National Research Council CNPq, and the Canadian NSERC Grant No. OGP0121756.

References

- [1] K. S. Novoselov, A. K. Geim, S. V. Morozov, D. Jiang, M.I. Katsnelson, I. V. Grigorieva, S. V. Dubonos, and A. A. Firsov, *Nature (London)* **438**, 197 (2005).
- [2] Y. Zheng, Y. W. Tan, H. L. Stormer, and P. Kim, *Nature (London)* **438**, 201 (2005).
- [3] M. I. Katsnelson, K. S. Novoselov, and A. K. Geim, *Nature Physics* **2**, 620 (2006); J. Milton Pereira Jr., P. Vasilopoulos, and F. M. Peeters, *Appl. Phys. Lett.* **90**, 132122 (2007).
- [4] F. M. Peeters and A. Matulis, *Phys. Rev. B* **48**, 15166 (1993).
- [5] J. Reijniers, F. M. Peeters, and A. Matulis, *Phys. Rev. B* **64**, 245314 (2001).
- [6] J. Reijniers, F. M. Peeters, and A. Matulis, *Phys. Rev. B* **59**, 2817(1999).
- [7] A. De Martino, L. Dell' Anna, and R. Egger, *Phys. Rev. Lett.* **98**, 066802 (2007).
- [8] M. Ramezani Masir, P. Vasilopoulos, A. Matulis, and F. M. Peeters, *Phys. Rev. B* **77**, 235443 (2008).
- [9] M. Ramezani Masir, P. Vasilopoulos, and F. M. Peeters, *Appl. Phys. Lett.* **93**, 242103 (2008).
- [10] S. Park and H. S. Sim, *Phys. Rev. B* **77**, 075433 (2008).
- [11] L. Oroszlany, P. Rakyta, A. Kormanyos, C.J. Lambert, and J. Cserti, *Phys. Rev. B* **77**, 081403(R) (2008).

- [12] T. K. Ghosh, A. De Martino, W. Häusler, L. Dell’Anna, and R. Egger, Phys. Rev. B **77**, 081404(R) (2008).
- [13] F. Zhai and K. Chang, Phys. Rev. B **77**, 113409 (2008).
- [14] M. Tahir and K. Sabeeh, Phys. Rev. B **77**, 195421 (2008).
- [15] Hengyi Xu, T. Heinzl, M. Evaldsson, and I.V. Zozoulenko, Phys. Rev. B **77**, 245401 (2008).
- [16] Cheol-Hwan Park, Feliciano Giustino, Marvin L. Cohen and Steven G. Louie Nano Lett. **9** , 1731, (2009).
- [17] H. van Houten, B. J. van Wees, J. E. Mooij, C. W. J. Beenakker, J. G. Williamson, and C. T. Foxon, Europhys. Lett. **5**, 721 (1988).
- [18] J. Spector, H. L. Stormer, K. W. Baldwin, L. N. Pfeiffer, and K. W. West, Appl. Phys. Lett. **56**, 1290 (1990).
- [19] U. Sivan, M. Heiblum, C. P. Umbach, and H. Shtrikman, Phys. Rev. B **41**, R7937 (1990).
- [20] L.W. Molenkamp, A. A. M. Staring, C.W. J. Beenakker, R. Eppenga, C. E. Timmering, J. G. Williamson, C. J. P. M. Harmans, and C. T. Foxon, Phys. Rev. B **41**, R1274 (1990).
- [21] A. Yacoby, M. Heiblum, V. Umansky, H. Shtrikman, and D. Mahalu, Phys. Rev. Lett. **73**, 3149 (1994).
- [22] A. Matulis, F. M. Peeters, and P. Vasilopoulos, Phys. Rev. Lett. **72**, 1518 (1994).
- [23] A. Nogaret, D. N. Lawton, D. K. Maude, J. C. Portal, and M. Henini, Phys. Rev. B **67**, 165317 (2003).
- [24] Vitor M. Pereira and Antonio H. Castro Neto, arXiv: 0810.4539v3 (2009).
- [25] S. Ghosh and M. Sharma, arXiv: 0806.2951 (2008).
- [26] L. Dell’Anna and A. D. Martino, Phys. Rev. B **79**, 045420 (2009).
- [27] I. S. Ibrahim and F. M. Peeters, Phys. Rev. B **52**, 17321 (1995); Am. J. Phys. **63**, 171 (1995).
- [28] Max Born and Emil Wolf, *Principles of Optics*, (Pergamon Press, 1980).
- [29] Amnon Yariv, *Optical Waves in Crystals*, (John Wile & Sons, Inc. 1976).
- [30] L. A. Ponomarenko, F. Schedin, M. I. Katsnelson, R. Yang, E. W. Hill, K. S. Novoselov and A. K. Geim, Science **320**, 356 (2008).
- [31] Vadim V. Cheianov, Vladimir Falko and B. L. Altshuler, Science **315**, 1252 (2007);
- [32] Bruce H. J. McKellar and G. J. Stephenson, Jr., Phys. Rev. C **35**, 2262 (1987).
- [33] David J. Griffiths and Carl A. Steinke. Am. J. Phys. **69** , 137 (2001);